Electronic Supplementary Material (ESI) for Dalton Transactions.

Regulating the electronic structure of $MoO_2/Mo_2C/C$ by heterostructure and oxygen vacancies for boosting lithium storage kinetics

Donglei Guo[a,1], Mengke Yang[a,b,1], Fang Wang[a], Yihua Cheng[a], Anqi Zhang[a], Guilong Liu[a], Naiteng Wu[a], Ang Cao[c], Hongyu Mi*[b] and Xianming Liu*[a]

[a] Key Laboratory of Function-oriented Porous Materials, College of Chemistry and Chemical Engineering, Luoyang Normal University, Luoyang, 471934, P. R. China.

*Email: myclxm@163.com

[b] State Key Laboratory of Chemistry and Utilization of Carbon Based Energy Resources, School of Chemical Engineering and Technology, Xinjiang University, Urumqi, 830046, P. R. China.

*Email: mmihongyu@163.com

[c] Department of Physics, Technical University of Denmark, Lyngby 2800, Denmark.

Experimental Section

Characterizations: X-ray diffraction (XRD), field-emission scanning electron microscope (FESEM, Sigma 500) and a H-8100 transmission electron microscopy (TEM) were employed to characterize the phase composition, structure and morphologies of as-prepared products. The energy dispersive spectrometer (EDS) and element maps were taken on a Sigma 500 FESEM unit. The Raman spectra were collected on an Invia Raman spectrometer with the excitation laser wave-length of 633 nm. The X-ray photoelectron spectra (XPS) were recorded on an ESCALAB 250 spectrometer (Perkin-Elmer). The electron paramagnetic resonances (EPR) were tested on a Bruker EMX Micro spectrometer at room temperature. The specific surface areas were calculated using a standard Brunauer-Emmett-Teller (BET) method on a Belsorp-max surface area detecting instrument. The thermo-gravimetric analysis (TGA) was carried out on a DTG-60AH instrument under the air flow. The photoluminescence (PL) spectra were obtained by using a Cary Eclipe florescence spectrometer (Varian, USA).

Electrochemical measurements: The assembly of CR2032 coin cells was carried in an argon-filled glove box with water and oxygen contents below 0.5 ppm. The free-standing $MoO_2/Mo_2C/C$ film was directly cut into the disk with the diameter of 1.2 cm as the working electrode. Lithium metal foil as counter electrode and 1 mol L^{-1} $LiPF_6$ solution with the mixture of EC: DEC: EMC at volume ratio of 1:1:1 as electrolyte. The charge-discharge profiles of the samples were determined by cycling in the potential range of 0.01-3 V at different current rates. Cyclic voltammetry measurements (CV, at different scanning rates) and electrochemical impedance spectroscopy (EIS, in the frequency range from 100,000 to 0.01 Hz) were investigated on a Parstat 4000+ workstation (Princeton Applied Research).

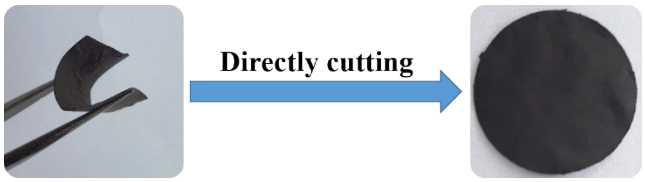

Fig. S1 Digital photographs of as-prepared $MoO_2/Mo_2C/C$ film and corresponding electrode disk.

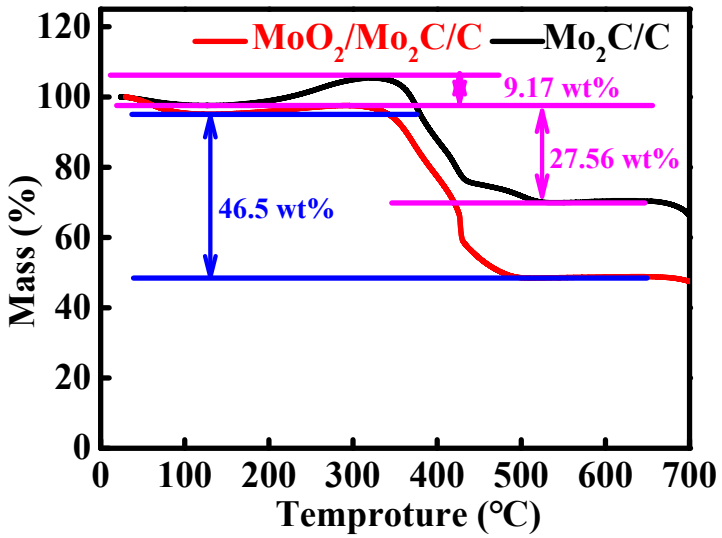

Fig. S2 TGA curves of $MoO_2/Mo_2C/C$ and Mo_2C/C.

The TGA analysis of $MoO_2/Mo_2C/C$ and Mo_2C/C was carried out to calculate the carbon content in $MoO_2/Mo_2C/C$. The Mo_2C/C and $MoO_2/Mo_2C/C$ samples were prepared from the same precursor and annealed temperature, just with different annealed time. The increasing mass of $MoO_2/Mo_2C/C$ is corresponded to the oxidation of MoO_2 and Mo_2C. The carbon content in $MoO_2/Mo_2C/C$ is determined to be about 50.4 wt% and the involved reaction as follows:

$2MoO_2 + O_2 = 2MoO_3$

$Mo_2C + 4O_2 = 2MoO_3$

$2MoO_2 + 3C = Mo_2C+CO_2$

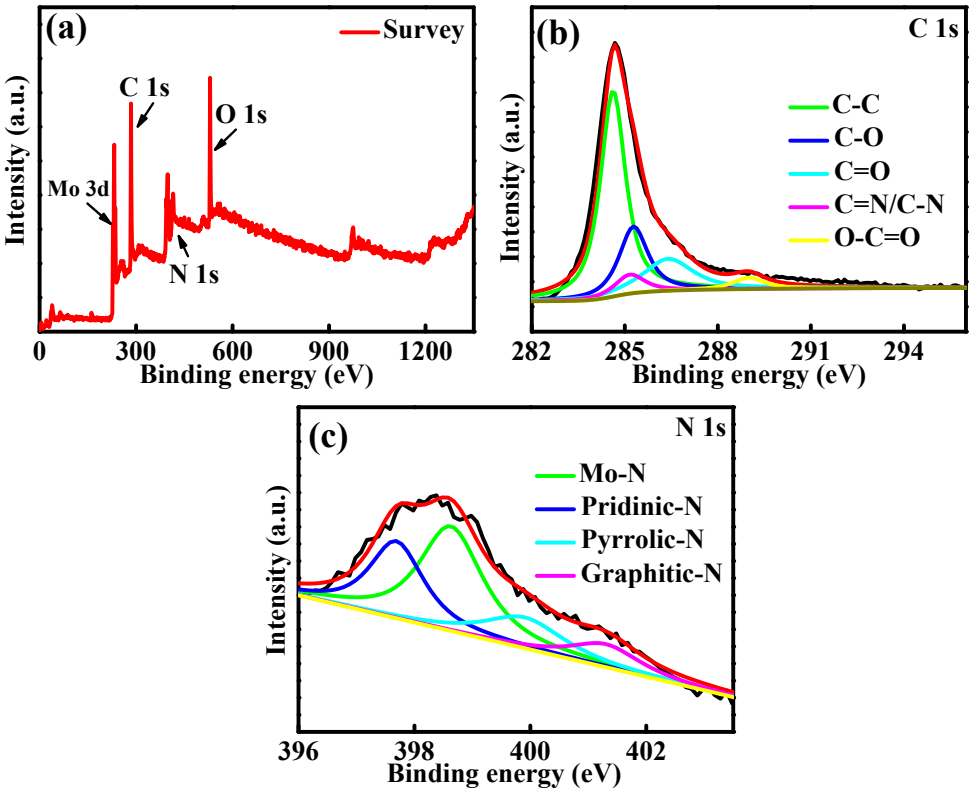

Fig. S3 (a) The XPS survey spectrum of $MoO_2/Mo_2C/C$. High-resolution XPS spectra of $MoO_2/Mo_2C/C$: (b) C 1s and (c) N1s.

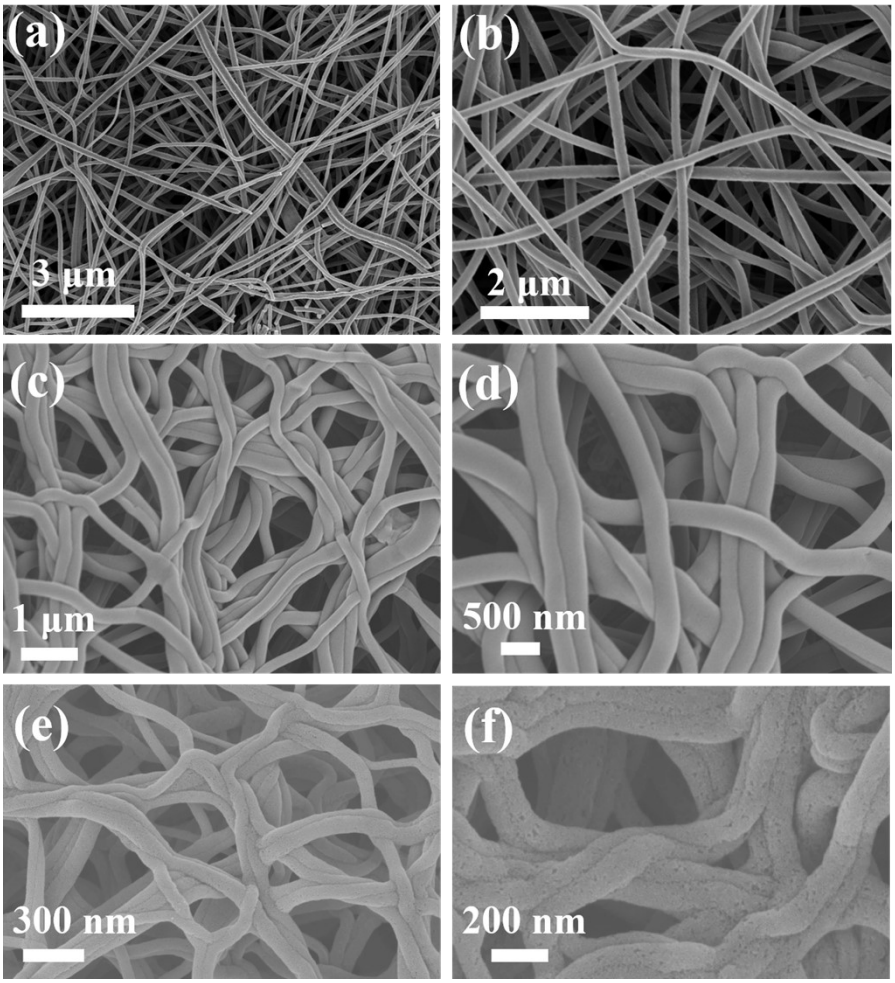

Fig. S4 (a, b) FESEM images of precursor. (c, d) FESEM images of MoO_2/C. (e, f) FESEM images of Mo_2C/C.

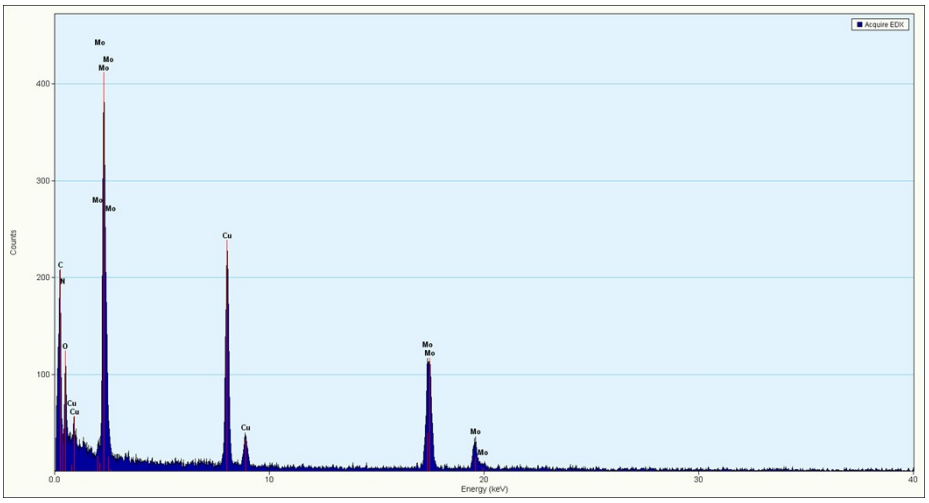

Fig. S5 The HAADF-STEM EDX image of $MoO_2/Mo_2C/C$.

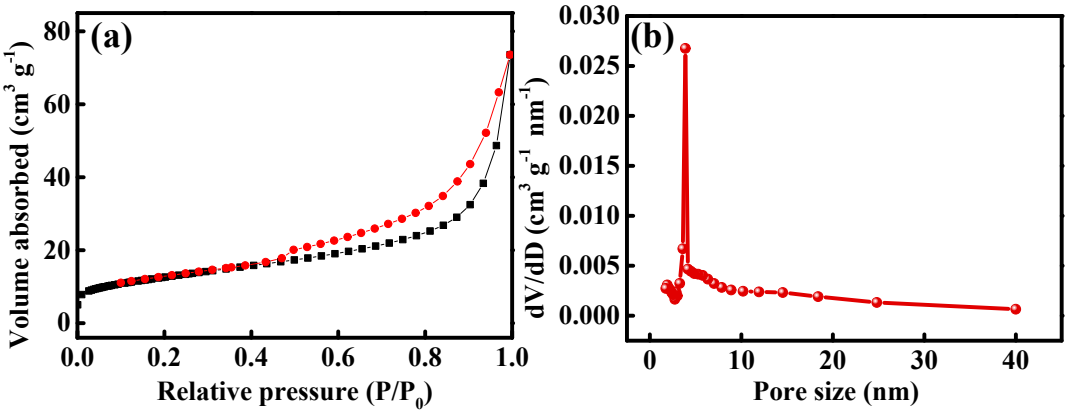

Fig. S6 N_2 adsorption-desorption isotherm (a) and pore size distribution (b) of $MoO_2/Mo_2C/C$ according to the NLDFT model.

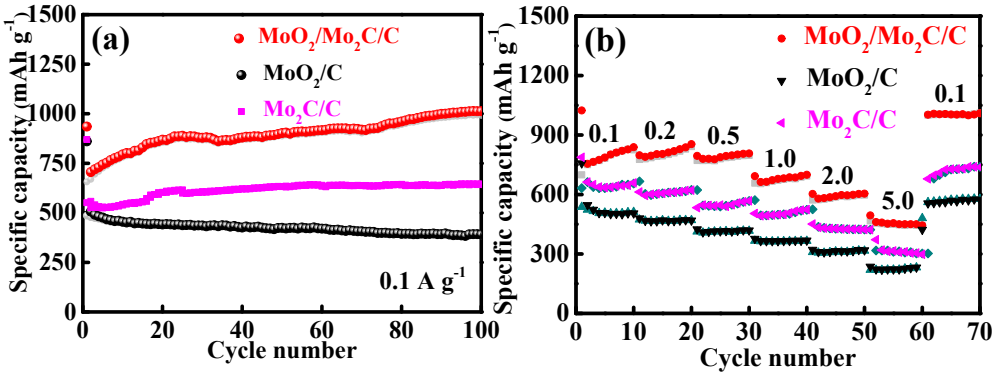

Fig. S7 Cyclic performance (a) and rate performance (b) of $MoO_2/Mo_2C/C$, MoO_2/C and Mo_2C/C.

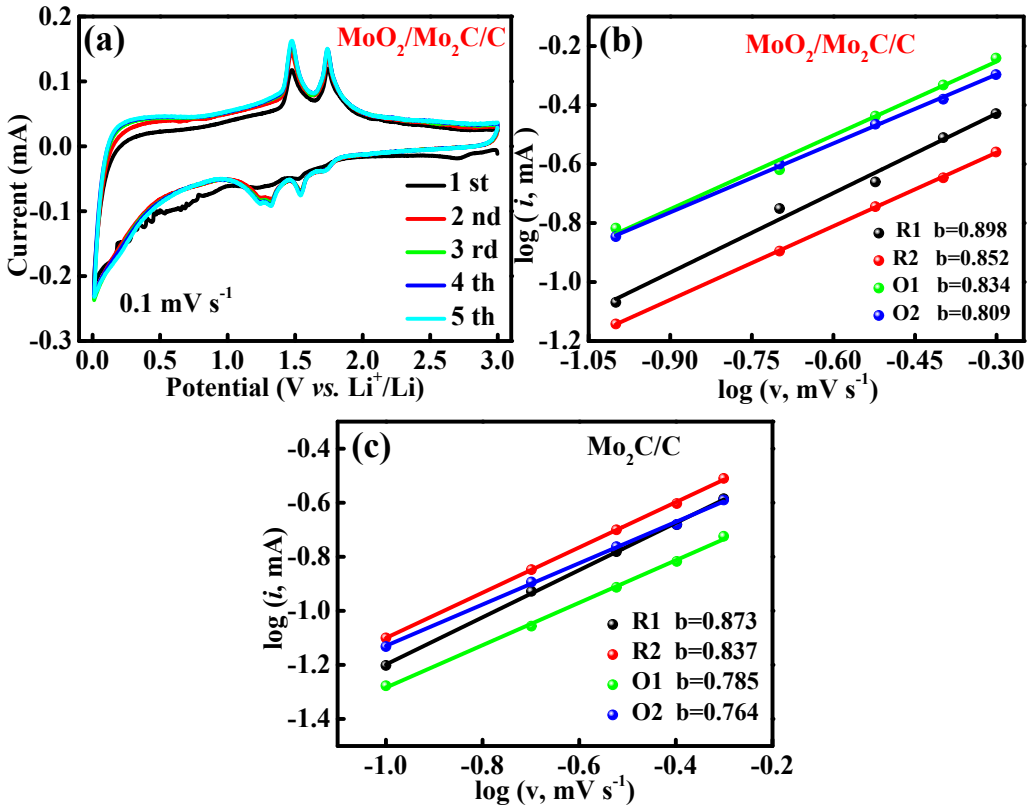

Fig. S8 (a) CV curves of $MoO_2/Mo_2C/C$ at a scan rate of 0.1 mV s^{-1}. (b) Log (i) versus log (v) plots at different oxidation and reduction states of $MoO_2/Mo_2C/C$. (c) Log (i) versus log (v) plots at different oxidation and reduction states of MoO_2/C.

.

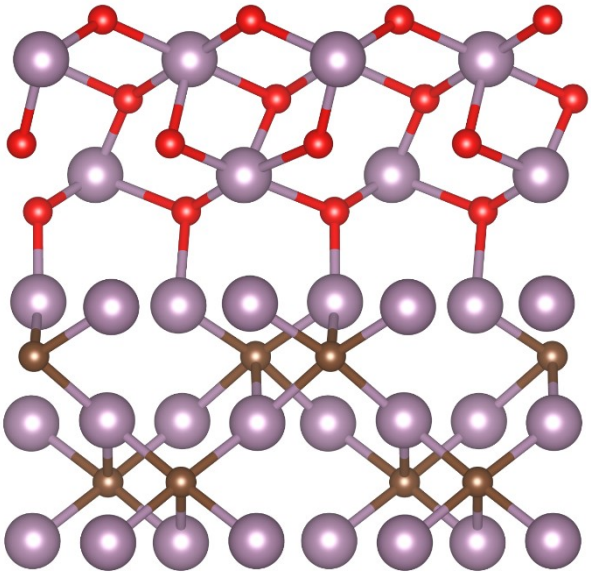

Fig. S9 Geometrically optimized models of MoO_2/Mo_2C heterointerface model.

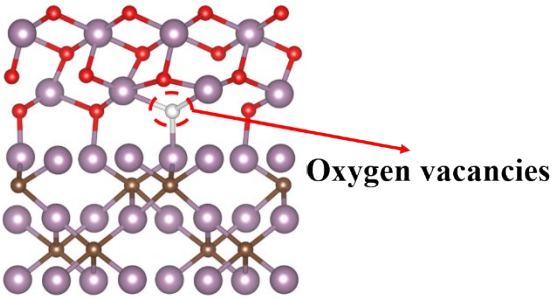

Fig. S10 Geometrically optimized model of MoO_2/Mo_2C with oxygen vacancies.

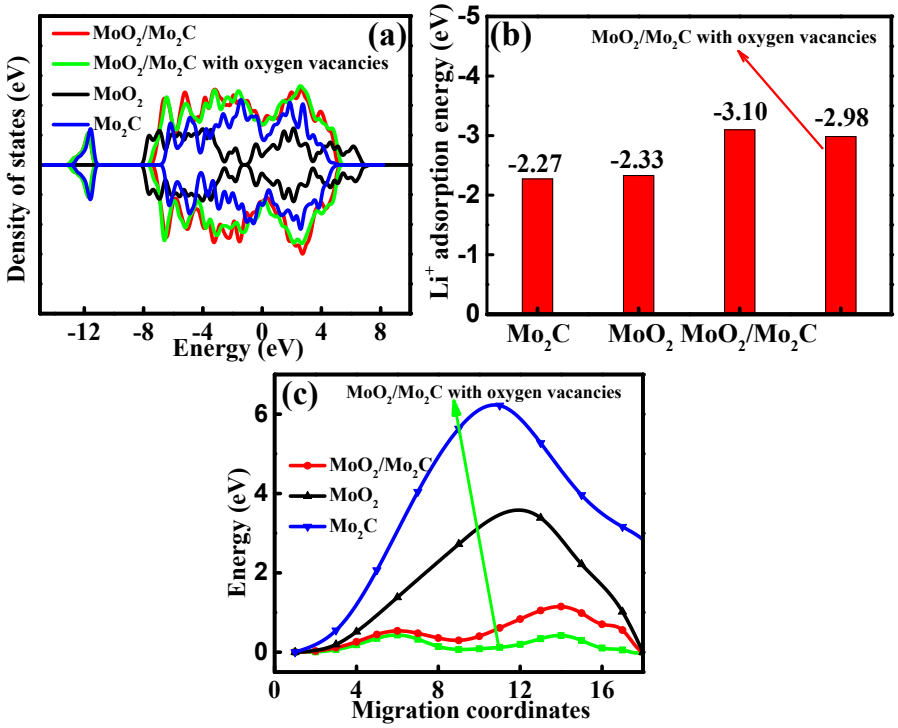

Fig. S11 Calculated DOS (a), adsorption energy of Li (b) and migration energy profiles (c) of MoO_2/Mo_2C heterostructures, MoO_2, Mo_2C and MoO_2/Mo_2C with oxygen vacancies models.

Table S1. Comparison of the electrochemical performance of the $MoO_2/Mo_2C/C$ with reported MoO_2-based anodes for LIBs.

MoO_2-based materials	Rate capability	Cyclic performance	Ref.
	Current density (A g^{-1})/Capacity (mA h g^{-1})	Current density (A g^{-1})/Cycle number/Capacity (mA h g^{-1})	
MoO_2@C	1/543	1/1000/443.8	[1]
MoO_2@NC	5/345	0.5/100/692.4	[2]
MoO_2/Ni/C	1/463	1/800/445	[3]
MoO_2/C	5/363.2	5/3000/193.5	[4]
MoO_2/NC NFs	10/291	1/600/720	[5]
MoO_2@RGO	2/473	1/50/523	[6]
MoO_2@C	2/312	1/600/537	[7]
MoO_2/Mo_2C/RGO	1/200	0.5/150/500	[8]
MoO_2/Mo_2N	5/415	0.1/100/815	[9]
$MoO_2/Mo_2C/C$	10/297.8	1/2400/507.3	[10]
MoO_2/MoP-NBs	8/291.2	1/1000/515	[11]
MoO_2@MoS_2	1/700	0.5/100/815	[12]
This work	5/454.7	2/1000/569	

References in Supporting Information

[1] G. L. Xia, F. C. Zheng, Y. Yang, J. W. Su and Q. W. Chen, *J. Mater. Chem. A*, 2016, **4**, 12434-12441.

[2] X. J. Tan, C. F. Cui, S. Q. Wu, B. C. Qiu, L. Z. Wang, J. L. Zhang, *Chem. Asian J*, 2017, **12**, 36-40.

[3] Q. Xia, H. L. Zhao, Z. H. Du, Z. J. Zhang, S. M. Li, C. H. Gao and K. Świerczek, *J. Mater. Chem. A*, 2016, **4**, 605-611.

[4] C. X. Hou, W. Y. Yang, X. B. Xie, X. Q. Sun, J. Wang, N. Naik, D. Pan, X. M. Mai, Z. H. Guo, F. Dang and W. Du, *J. Colloid Interface. Sci.*, 2021, **596**, 396-407.

[5] J. J. Liang, X. Gao, J. Guo, C. M. Chen, K. Fan and J. M. Ma, *Sci. China Mater.*, 2018, **61**, 30-38.

[6] X. C. Chen, R. P. Liu, L. X. Zeng, X. X. Huang, Y. X. Fang, J. B. Liu, Y. X. Xu, Q. H. Chen, M. D. Wei and Q. R. Qian, *Mater. Lett.*, 2017, **212**, 198-201.

[7] Z. Chen, T. Yang, H. M. Shi, T. H. Wang, M. Zhang and G. Z. Cao, *Adv. Mater. Interfaces*, 2017, **4**, 1600816.

[8] W. Devina, J. Hwang and J. Kim, *Chem. Eng. J.*, 2018, **345**, 1-12.

[9] J. Liu, S. S. Tang, Y. K. Lu, G. M. Cai, S. Q. Liang, W. J. Wang and X. L. Chen, *Energy Environ. Sci.*, 2013, **6**, 2691-2697.

[10] C. X. Hou, J. Wang, W. Du, J. C. Wang, Y. Du, C. T. Liu, J. X. Zhang, H. Hou, F. Dang, L. L. Zhao and Z. H. Guo, *J. Mater. Chem. A*, 2019, **7**, 13460-13472.

[11] Y. H. Shen, Y. L. Jiang, Z. Z. Yang, J. Dong, W. Yang, Q. Y. An and L. Q. Mai, *Adv. Sci.*, 2022, **9**, 2104504.

[12] Z. N. Deng, Y. J. Hu, D. Y. Ren, S. L. Lin, h. Jiang and C. Z. Li, *Chem. Commun.*, 2015, **51**, 13838-13841.